

SUPERACID $ZrO_2-SiO_2-SnO_2$ MIXED OXIDE: SYNTHESIS AND STUDY

Svitlana Prudius^{1, ✉}, Natalia Hes¹, Volodymyr Trachevskiy²,
Oleg Khyzhun³, Volodymyr Brei¹

<https://doi.org/10.23939/chcht15.03.336>

Abstract. Superacid ternary $ZrO_2-SiO_2-SnO_2$ oxide has been synthesized by the sol-gel method with a different atomic ratio Zr:Si:Sn. The highest strength of acid sites has been observed in the ranges of $20 \leq Zr^{4+} \leq 29$, $60 \leq Si^{4+} \leq 67$, $11 \leq Sn^{4+} \leq 20$ at. %. According to the XPS spectra and ^{119}Sn , ^{29}Si MAS NMR spectra of $ZrO_2-SiO_2-SnO_2$ a partial shift of electron density from zirconium to silicon ions was observed resulting in the formation of superacid Lewis sites. It was shown that superacid $Zr_{29}Si_{60}Sn_{11}$ mixed oxide efficiently catalyzes acylation of toluene with acetic anhydride at 423 K in a flow reactor with 45% conversion of anhydride at 100 % selectivity towards *p*-methylacetophenone.

Keywords: solid superacid, ternary oxide, tin dioxide, acid strength, Lewis sites.

1. Introduction

Solid acids have been always considered as promising low-temperature catalysts for such processes as isomerization of C_{4-7} *n*-alkanes and alkylbenzenes [1], acylation, nitration and rearrangement of aromatic compounds, where strong acid sites ($H_0 < -12$) are required. Sulfated ($H_0 = -16.04$) and tungstated ($H_0 = -14.52$) zirconia, discovered by Hino and Arata, are well-known and studied superacids [2, 3]. Sulfated zirconia was applied in an industry for isomerization of *n*-butane into isobutane at 373 K [4]. Since then, several types of new superacids are constantly being proposed. A new class of solid superacids based on the sulfated metal-organic framework have been prepared and studied [5]. For

instance, superacidic $Zr_6O_5(OH)_3(1,3,5\text{-benzenetricarboxylate})_2(SO_4)_{2.5}(H_2O)_{2.5}$ with $H_0 = -14.52$ provides effective acylation of anisole and isomerization of α -pinene at moderate temperatures (383–333 K) [6]. Recently, the new hierarchically porous Brønsted superacid material synthesized by grafting sulfonic acid groups on a highly fluorinated porous polymer framework (FPOP- SO_3H) was presented [7]. The resultant material ($H_0 = -12.4$) has a much higher surface area and accessible H^+ content than the benchmark Nafion® NR50.

As was shown in [8, 9], the acidity of binary mixed oxides can be increased by doping with a third element. So, the authors [9] have found that at a doping of ZrO_2-SiO_2 with Al^{3+} ions, the strength of acid sites of ternary $ZrO_2-SiO_2-Al_2O_3$ oxide increases by three order from $H_0 = -11.35$ to -14.52 . In this work we have exchanged Al^{3+} on Sn^{4+} ions in synthesis of the ternary mixed oxide. The binary ZrO_2-SiO_2 mixed oxide with strong and moderate acid sites ($H_0 = -11.35$) is of considerable interest due to its unique properties such as mechanical and chemical resistance, high specific surface area, and a porous structure [10]. The SnO_2-SiO_2 and SnO_2-ZrO_2 mixed oxides, according to Tanabe's rule, also are acid materials less strong than ZrO_2-SiO_2 [11, 12].

In this communication the data on synthesis and acidity of $ZrO_2-SiO_2-SnO_2$ samples with different Zr:Si:Sn ratios are presented. The formation of superacid sites on the surface of $ZrO_2-SiO_2-SnO_2$ is discussed. The results on catalytic activity of obtained oxide in acylation of toluene with acetic anhydride are presented also.

2. Experimental

The $ZrO_2-SiO_2-SnO_2$ samples with different Zr:Si:Sn ratios have been synthesized by a sol-gel method. Zirconyl chloride $ZrOCl_2 \cdot 8H_2O$, tetraethyl-orthosilicate (TEOS) and tin (IV) chloride pentahydrate $SnCl_4 \cdot 5H_2O$ were used as starting chemicals. The $ZrO_2-SiO_2-SnO_2$ samples were denoted as $Zr_xSi_ySn_z$, where *x*, *y* and *z* represented the atomic percentage of cations. The

¹Institute of Sorption and Problems of Endoecology of the NAS of Ukraine, Kyiv, Ukraine,

13, General Naumov Str., 03164, Kyiv, Ukraine

²Technical Center of the NAS of Ukraine, Kyiv, Ukraine,
13, Pokrovska Str., 04070, Kyiv, Ukraine

³Frantsevich Institute for Problems of Materials Science of the NAS of Ukraine, Kyiv, Ukraine

3, Krzhizhanovsky Str., 03142, Kyiv, Ukraine,

✉ svitprud@gmail.com

© Prudius S., Hes N., Trachevskiy V., Khyzhun O., Brei V., 2021

following is a typical sample synthesis procedure using the Zr₂₉Si₆₀Sn₁₁ sample as an example. 50 ml of an aqueous solution containing 10.56 g of zirconium oxychloride and 4.37 g of tin dioxide was added to 50 ml of solution containing mixture of 14.13 g TEOS, ethanol and water (TEOS:C₂H₅OH:H₂O = 15:8:77 wt %). Then, 20.4 g of urea was added under stirring. The sol was aged for two days at 366 K. The gel was washed, dried at 393 K and calcined at 1023 K for 2 h. Also, pure SiO₂, ZrO₂ and SnO₂ samples were synthesized by the same procedure.

Total acidity of all samples was determined by reverse titration using *n*-butylamine solution in cyclohexane and bromthymol blue as an indicator. The strength of acid sites and concentration-strength acid site distribution were estimated using Hammett indicators (Aldrich): benzalacetophenone (pK_{BH+} = -5.6), anthraquinone (-8.2), 4-nitrotoluene (-11.35), 1-chloro-3-nitrobenzene (-13.16), 2,4-dinitrotoluene (-13.75) and 2,4-dinitro-1-fluorobenzene (-14.52). All samples were dried at 823 K for 1 h before testing [11].

Specific surface area, total pore volume and average pore radius of the samples were calculated from N₂ adsorption-desorption isotherms obtained on a Quantachrome Nova 2200e Surface Area and a Pore Size Analyzer. The X-ray powder diffraction analysis of obtained samples was performed with a DRON-4-07 diffractometer (CuKα).

The diffuse reflectance ultraviolet-visible (UV-Vis) spectra of the samples were recorded in air against BaSO₄ at 200–700 nm using a Shimadzu UV-2450 spectrophotometer. In order to determine the forbidden gap energy *E*₀, the reflectance spectra were recalculated to absorption spectra using Kubelka-Munk formula, $F = (h\nu(1-R)^2/2R)^{1/2}$. *E*₀ values were determined from the nearly linear long-wave segment of absorption band plot extrapolated to interception with abscissa [13].

The ¹¹⁹Sn and ²⁹Si MAS NMR spectra were recorded employing a Bruker Avance 400 (Karlsruhe, Germany) spectrometer at 149.5 and 79.5 MHz with a sample spinning rate at magic angle of 7 kHz. The shifts are referenced with respect to H₂SnCl₄.

The XPS spectra were registered with a UHV-Analysis System (SPECS Surface Nano Analysis Company, Berlin, Germany) equipped with PHOIBOS-150 energy analyzer. The spectrometer energy scale was calibrated using pure etalon gold and copper metals as described elsewhere [14] and the spectra were excited by Mg K_α source (*E* = 1253.6 eV, *P*_{max} = 100 W). Charging effects were verified in reference to the C 1s line (284.6 eV) of hydrocarbon adsorbed on the sample surface as recommended for such kinds of materials [15].

Catalytic activity of ZrO₂-SiO₂-SnO₂ samples was tested in the reaction of toluene (PhMe) acylation with acetic anhydride (AA) (PhMe:AA = 10:1, mole). The experiments were carried out in a vertical down-flow glass reactor (*d* = 7 mm) with fixed bed of a catalyst (1.5 cm³, 0.8 g) at 423 K in Ar flow (3 ml/min). The liquid reaction mixture was introduced into reactor using an Orion M 361 syringe pump at LHSV = 0.7 h⁻¹, that correspond to load on a catalyst of 0.6 mmol AA/g_{cat}/h. The condensed reaction products were analyzed using gas chromatography (Chrom-5 with 50 m capillary column) method.

3. Results and discussion

For studying the composition effect of ZrO₂-SiO₂-SnO₂ mixed oxide on its acid strength, 25 samples have been synthesized with different ratios of Zr_{*x*}Si_{*y*}Sn_{*z*}, where *x*, *y* and *z* represented the atomic percentage of cations. The results are presented in ternary diagram (Fig. 1) and Table 1.

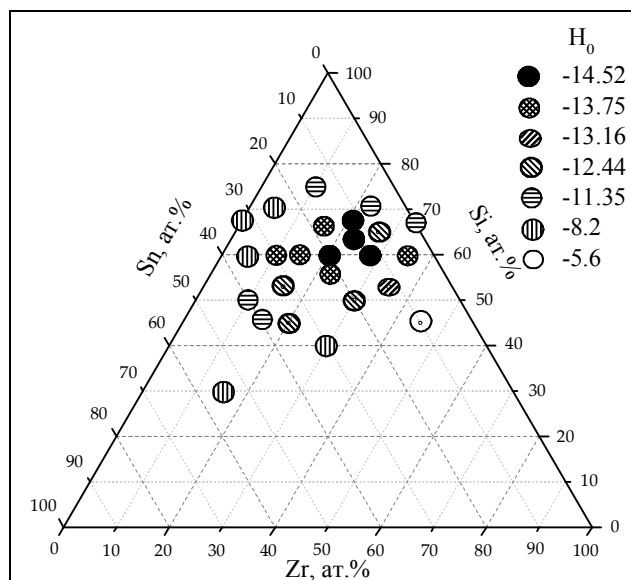


Fig. 1. Effect of Zr:Si:Sn ratio on acid strength of ZrO₂-SiO₂-SnO₂

Maximal strength of acid sites (*H*₀ = -14.52) is observed for samples with 20 ≤ Zr⁴⁺ ≤ 29, 60 ≤ Si⁴⁺ ≤ 67, 11 ≤ Sn⁴⁺ ≤ 20 at.%. The total acidity for these samples is at the level of 1.1–1.6 mmol/g. The samples have high specific surface area (340–415 m²/g) and wide pore diameter (2.5–3.2 nm) (Table 1). The superacid region with *H*₀ ≥ -12.44 is limited to the cations concentrations of 10 ≤ Zr⁴⁺ ≤ 35, 45 ≤ Si⁴⁺ ≤ 67 and 5 ≤ Sn⁴⁺ ≤ 35% (Fig. 1, Table 1).

Textural and acid parameters of superacid $\text{ZrO}_2\text{-SiO}_2\text{-SnO}_2$ samples

Sample	Specific surface area, m^2/g	Pore volume, cm^3/g	Average pore diameter, nm	Total acidity, mmol/g	Acid strength, H_0
$\text{Zr}_{21}\text{Si}_{67}\text{Sn}_{11}$	360	0.26	3.0	1.6	-14.52
$\text{Zr}_{20}\text{Si}_{60}\text{Sn}_{20}$	415	0.33	3.2	1.6	-14.52
$\text{Zr}_{29}\text{Si}_{60}\text{Sn}_{11}$	340	0.20	2.4	1.5	-14.52
$\text{Zr}_{23}\text{Si}_{64}\text{Sn}_{13}$	340	0.21	2.5	1.1	-14.52
$\text{Zr}_{23}\text{Si}_{55}\text{Sn}_{22}$	300	0.19	2.5	1.4	-13.75
$\text{Zr}_{35}\text{Si}_{60}\text{Sn}_5$	370	0.23	2.5	1.4	-13.75
$\text{Zr}_{15}\text{Si}_{60}\text{Sn}_{25}$	290	0.19	2.6	1.4	-13.75
$\text{Zr}_{10}\text{Si}_{60}\text{Sn}_{30}$	260	0.19	3.0	0.9	-13.75
$\text{Zr}_{16}\text{Si}_{66}\text{Sn}_{18}$	280	0.19	2.7	1.5	-13.75
$\text{Zr}_{35}\text{Si}_{53}\text{Sn}_{12}$	290	0.17	2.4	1.1	-13.16
$\text{Zr}_{10}\text{Si}_{50}\text{Sn}_{40}$	280	0.25	3.6	1.5	-12.44
$\text{Zr}_{20}\text{Si}_{45}\text{Sn}_{35}$	240	0.15	2.6	1.0	-12.44
$\text{Zr}_{30}\text{Si}_{50}\text{Sn}_{20}$	250	0.16	2.6	1.3	-12.44
$\text{Zr}_{15}\text{Si}_{53}\text{Sn}_{32}$	270	0.18	2.7	1.5	-12.44
$\text{Zr}_{27}\text{Si}_{65}\text{Sn}_8$	340	0.21	2.4	1.4	-12.44

The results on strength acid site distribution for prepared $\text{Zr}_{20}\text{Si}_{60}\text{Sn}_{20}$ sample are presented in Fig. 2. The wide range of acid strength, from 40% medium ($-8.2 \geq H_0 \geq -12.14$) up to 10% superacidic value of $H_0 = -14/52$, is observed.

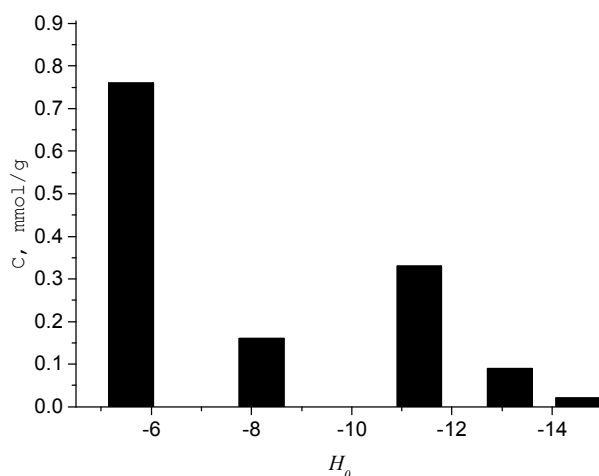


Fig. 2. Concentration-strength acid site distribution for $\text{Zr}_{29}\text{Si}_{60}\text{Sn}_{11}$ sample

According to the X-ray analysis (Fig. 3), the superacid $\text{ZrO}_2\text{-SiO}_2\text{-SnO}_2$ samples, with Zr^{4+} and $\text{Sn}^{4+} \leq 35$ at.%, are amorphous: halo maxima at 30° and 51° correspond to the most intense peaks for tetragonal ZrO_2 ($2\theta = 30.2^\circ$ and 50.8°). In samples with higher content of tin dioxide (already at $\text{Sn}^{4+} \geq 40$ at.%),

characteristic peaks are observed at $2\theta = 26.6^\circ$; 33.9° ; 38.0° and 51.8° that correspond to tetragonal SnO_2 with rutile structure [16] (Fig. 3).

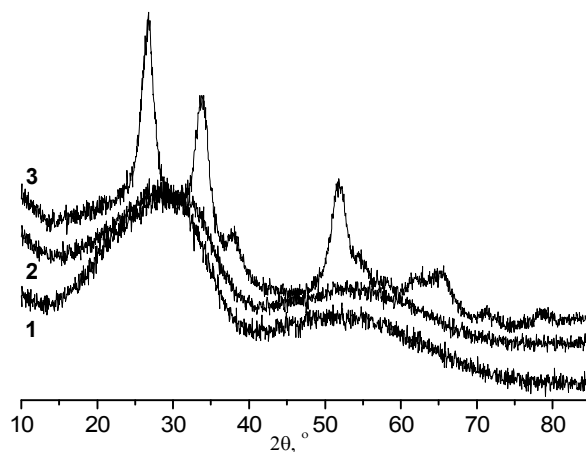


Fig. 3. XRD patterns of $\text{Zr}_{29}\text{Si}_{60}\text{Sn}_{11}$ (1), $\text{Zr}_{20}\text{Si}_{45}\text{Sn}_{35}$ (2) and $\text{Zr}_{15}\text{Si}_{45}\text{Sn}_{40}$ (3) samples after calcinations at 1023 K for 2 h

According to the UV-Vis spectra (Fig. 4a), isolated IVSn^{4+} (206 nm) or VISn^{4+} (220 nm) ions with different oxygen coordination are present in all studied samples. For samples with $11 \leq \text{Sn}^{4+} \leq 25$ at.% the maximum intensity is observed at ~ 200 nm that attributed to isolated tetrahedral IVSn^{4+} ions [16]. But the samples with $\text{Sn}^{4+} \geq 40$ at.% show a broad line around

260–300 nm that corresponds to octahedral $^{VI}Sn^{4+}$ ions in SnO_2 phase [16] (Fig. 4a) which is in agree with XRD data. So it is obvious that further growth of tin content leads to the formation of cassiterite phase.

Fig. 4b illustrates the optical band gap (E_g) for some $ZrO_2-SiO_2-SnO_2$ samples. It is known [17] that E_g value for massive SnO_2 is near 3.55 eV that close to the band gap of $Zr_{15}Si_{45}Sn_{40}$ sample (Fig. 4b). The E_g values, calculated for studied samples, increase from 3.6 to 4.4 eV at decreasing of tin content (Fig. 4b). As shown in [8], superacid WO_3/ZrO_2 samples are characterized by the band gap in the range 3.0–3.2 eV. Superacid $ZrO_2-SiO_2-SnO_2$ samples have the band gap at 3.9–4.3 eV (Fig. 4b).

In ^{119}Sn MAS NMR spectrum of $Zr_{29}Si_{60}Sn_{11}$ sample two signals at –650 and –570 ppm are observed

that obviously correspond to $^{VI}Sn^{4+}$ and $^{IV}Sn^{4+}$ ions in its matrix (Fig. 5a) [18]. Nuclei of ^{119}Sn are sensitive to change of oxygen coordination number in oxide framework. So, $^{IV}Sn^{4+}$ ions incorporated in zeolite framework have $\delta = -444$ ppm [18], and $^{VI}Sn^{4+}$ in SnO_2 (cassiterite) $\delta = -604$ ppm (Fig. 5a). The $Zr_{29}Si_{60}Sn_{11}$ signal is centered at –650 ppm (Fig. 5a), and the high-field shift on 50 ppm indicates the increase of electron density on ^{119}Sn nuclei compared to bulk SnO_2 .

^{29}Si MAS NMR spectrum of $Zr_{29}Si_{60}Sn_{11}$ sample shows a broadening and low-field shift on 9 ppm of the Q_4 signal to –107 ppm comparing to the peak of pure SiO_2 at –98 ppm, that indicates the increase of electron density on ^{29}Si nuclei with paramagnetic chemical shift (Fig. 5b). Similar shift was observed in ^{29}Si MAS NMR spectra of $Zr_{35}Si_{53}Al_{12}$ mixed oxide [9].

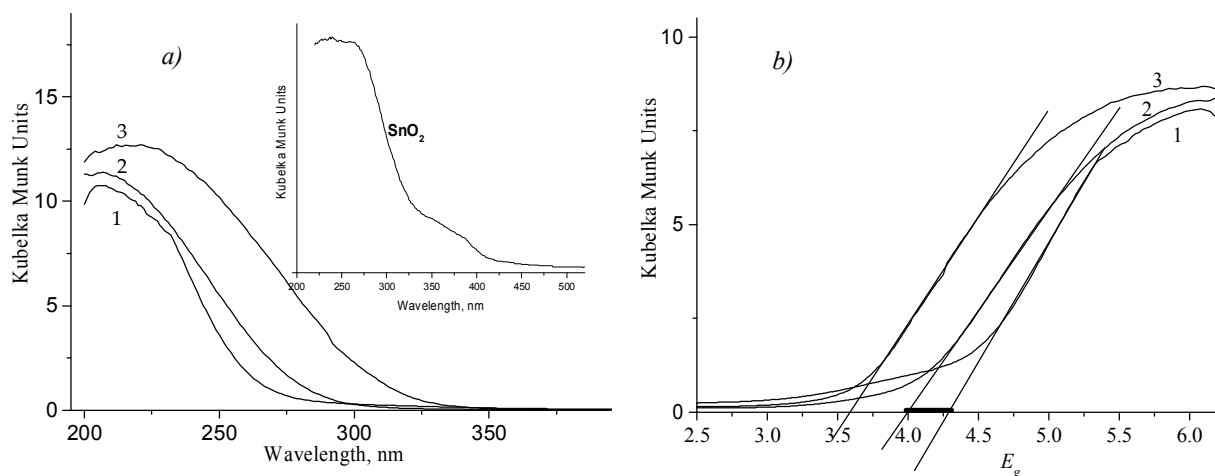


Fig. 4. UV-Vis diffuse reflectance spectra (a) and optical energy band gap (b) of $Zr_{29}Si_{60}Sn_{11}$ (1); $Zr_{15}Si_{60}Sn_{25}$ (2) and $Zr_{15}Si_{45}Sn_{40}$ (3)

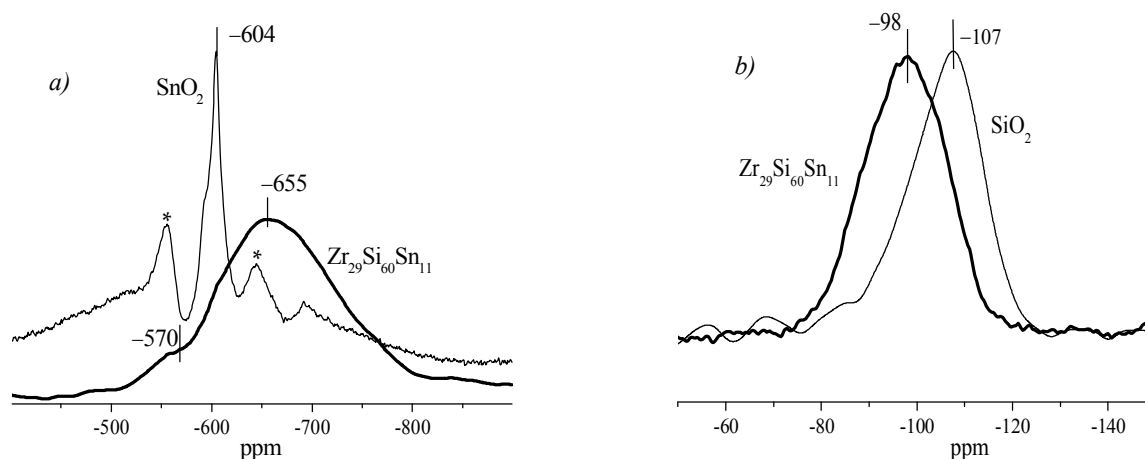


Fig. 5. ^{119}Sn MAS NMR spectra of $Zr_{29}Si_{60}Sn_{11}$ and SnO_2 (a); $Zr_{29}Si_{60}Sn_{11}$ and SiO_2 (b)

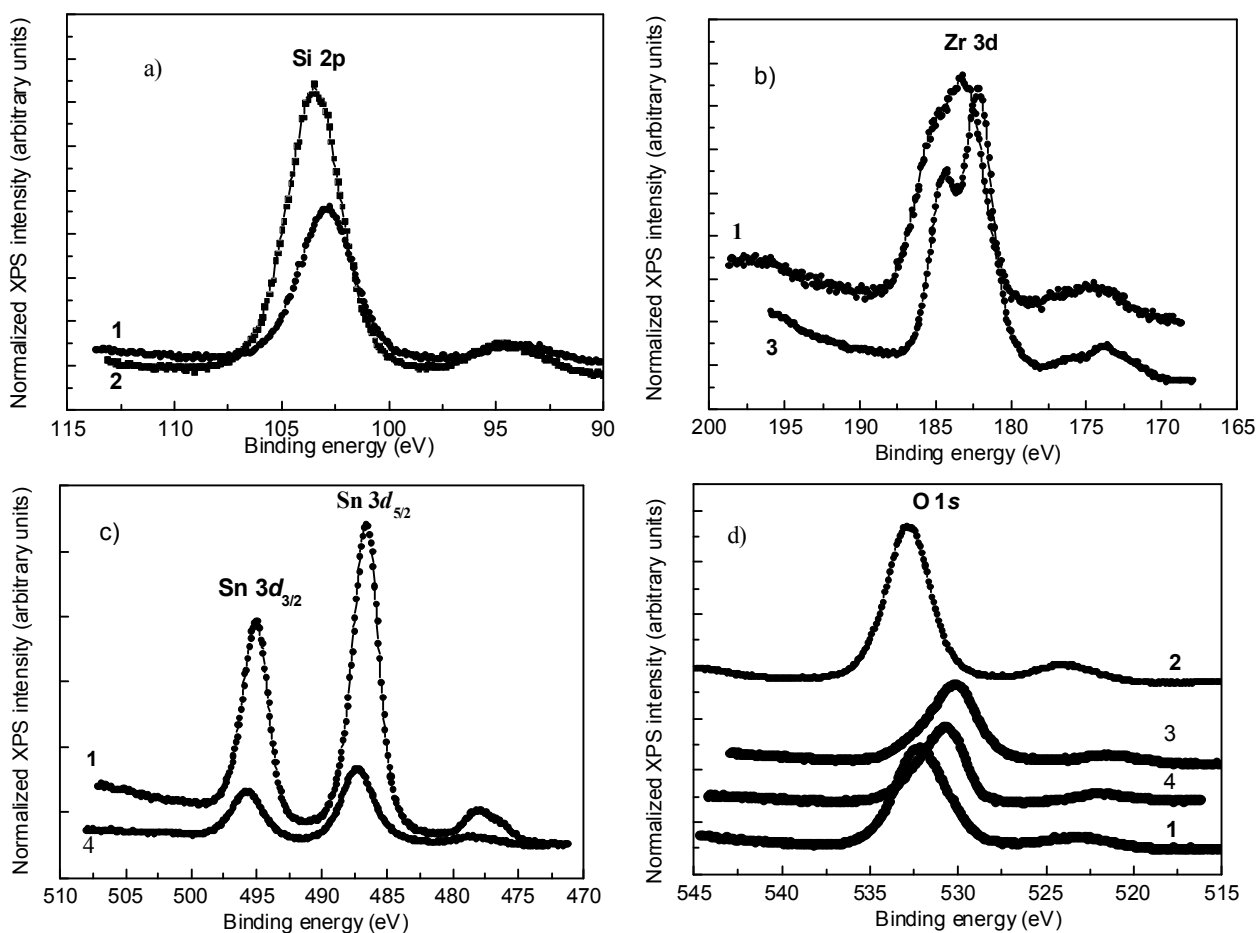


Fig. 6. XPS core-level Si 2*p* (a), Zr 3*d* (b), Sn 3*d* (c) and O 1*s* (d) spectra of the samples studied: $Zr_{20}Si_{60}Sn_{20}$ (1), SiO_2 (2), ZrO_2 (4) and SnO_2 (4)

Table 2

Measured binding energies (uncertainty is ± 0.1 eV) of Zr 3*d*, Si 2*p*, Sn 3*d* and O 1*s* core-level electrons of $Zr_{20}Si_{60}Sn_{20}$, ZrO_2 , SiO_2 and SnO_2

Sample	Zr 3 <i>d</i> _{5/2}	Si 2 <i>p</i> _{3/2}	Sn 3 <i>d</i> _{5/2}	O 1 <i>s</i>
$Zr_{20}Si_{60}Sn_{20}$	183.1	102.7	487.4	532.0
ZrO_2	182.3	-	-	530.2
SiO_2	-	103.5	-	532.9
SnO_2	-	-	486.7	530.7

The XPS core-level Zr 3*d*-, *p*-, Sn 3*d*- and O 1*s* spectra of the $Zr_{20}Si_{60}Sn_{20}$ sample and pure ZrO_2 , SiO_2 and SnO_2 oxides are shown in Fig. 6.

The corresponding binding energies are summarized in Table 2. The obtained binding energy of Zr 3*d*, Si 2*p* and Sn 3*d* core-level electrons of ZrO_2 , SiO_2 and SnO_2 correspond well to literature data for those oxides [19]. The Zr 3*d*_{5/2} and Sn 3*d*_{5/2} peaks positions for $Zr_{20}Si_{60}Sn_{20}$ are shifted towards higher binding energies comparing to that of pure ZrO_2 and SnO_2 , respectively,

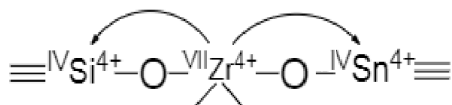
while binding energy of the Si 2*p*_{3/2} core-level spectrum is smaller in $Zr_{20}Si_{60}Sn_{20}$ than in pure SiO_2 oxide (Fig. 6, Table 2). Similar high-energy shift of Zr 3*d*_{5/2} peak in the XPS spectra of zircon ($ZrSiO_4$) was detected by Guittet *et al.* [20].

Observed shifts indicate that the electron density transfers from zirconium and tin atoms to silicon atoms in the $Zr_{20}Si_{60}Sn_{20}$ sample that is in agreement with data in the ^{29}Si MAS NMR spectra but not agreed with the ^{119}Sn MAS NMR spectra (Fig. 4). Noteworthy, the

¹¹⁹Sn MAS NMR spectrum of Zr₂₀Si₆₀Sn₂₀ reflects the change of electronic density on tin atoms in oxide matrix whereas the XPS spectrum – at surface layer only.

From Fig. 6 and data tabulated in Table 2, it is obvious that binding energy value of the XPS O 1s spectrum of SiO₂ is much bigger than those of ZrO₂ and SnO₂. This fact could be explained by different ionicity degree of the chemical bonding in these dioxides. In the Zr₂₀Si₆₀Sn₂₀ sample, the binding energy of the O 1s core-level electrons is smaller by 0.9 eV as compared to that of SiO₂, however it is bigger by 1.8 and 1.3 eV than those of ZrO₂ and SnO₂ (see Fig. 6 and Table 1). As a whole, O²⁻ anions in Zr₂₀Si₆₀Sn₂₀ matrix are characterized by the higher electronic density than in SiO₂.

On the basis of obtained UV-Vis, NMR and XPS data we suppose that induced positive charge on zirconium ions in ZrO₂-SiO₂-SnO₂ could form the strong L-sites ($H_0 = -14.52$) of such structure:



The activity of the superacid Zr₂₉Si₆₀Sn₁₁ oxide was tested in the acylation of toluene with acetic anhydride. It is known that strong acid sites ($pK_{BH^+} = -11.0$) are required for the formation of reactive acyl cations from carboxylic acids or their anhydrides [4]. The acylation reactions are slow enough, so they are usually studied under steady-state conditions, such as stirring a solution of acylation agent in toluene over a solid catalyst in autoclaves [21]. In this work, the acylation reaction was carried out using a flow reactor with a fixed catalyst bed. The superacid Zr₂₉Si₆₀Sn₁₁ catalyst provides 45% anhydride conversion with ~100% *p*-methylacetophenone selectivity at 423 K under load on a catalyst of 0.6 mmol AA/g_{cat}/h. The similar result was obtained on less acidic H-Beta zeolite in an autoclave at 423 K and reaction time of 4 h [21]. The regeneration of spent Zr₂₉Si₆₀Sn₁₁ catalyst at 773 K for 2 h fully restores its activity.

4. Conclusions

The acidity of mixed ZrO₂-SiO₂-SnO₂ oxide depends on the Zr:Si:Sn ratio. The highest strength ($H_0 = -14.52$) and content (1.6 – 1.1 mmol/g) of acid sites are observed for samples with $20 \leq Zr^{4+} \leq 29$, $60 \leq Si^{4+} \leq 67$, $11 \leq Sn^{4+} \leq 20$ at.%.

According to the diffuse UV-Vis reflectance spectra, ^{IV}Sn⁴⁺ and ^{VI}Sn⁴⁺ ions are present in ZrO₂-SiO₂-

SnO₂ framework. The determined limiting band gap of 3.9–4.3 eV is the criterion for superacid ZrO₂-SiO₂-SnO₂ synthesis. The low- and high-field chemical shifts in ²⁹Si and ¹¹⁹Sn MAS NMR spectra of Zr₂₉Si₆₀Sn₁₁ in comparison with pure SiO₂ and SnO₂ were detected, that indicates increasing electronic density on Si⁴⁺ and Sn⁴⁺ ions. Observed high-energy shifts of the Zr 3d_{5/2} and Sn 3d_{5/2} peaks of the XPS spectra indicate the electron density transfer from zirconium and tin to silicon atoms in Zr₂₀Si₆₀Sn₂₀ sample. Superacidity of ZrO₂-SiO₂-SnO₂ could be explained by the formation of coordination-unsaturated Zr⁴⁺ ions at the surface layer as strong Lewis sites. It was determined that superacid Zr₂₉Si₆₀Sn₁₁ mixed oxide effectively catalyzes the acylation of toluene with acetic anhydride at 423 K with nearly 100% selectivity towards *p*-methylacetophenone.

References

- [1] Patrylak L., Krylova M., Pertko O. *et al.*: Chem. Chem. Technol., 2020, **14**, 234. <https://doi.org/10.23939/chcht14.02.234>
- [2] Arata K.: Adv. Catal., 1990, **37**, 165. [https://doi.org/10.1016/S0360-0564\(08\)60365-X](https://doi.org/10.1016/S0360-0564(08)60365-X)
- [3] Arata K., Matsuhashi H., Hino M., Nakamura H.: Catal. Today, 2003, **81**, 17. [https://doi.org/10.1016/S0920-5861\(03\)00098-1](https://doi.org/10.1016/S0920-5861(03)00098-1)
- [4] Zazhigalov V., Strelko V., Khalamejda S. *et al.*: Proceedings of the DGMK-Conference "C4/C5-Hydrocarbons: Routes to Higher Value-Added Products", 2004, 209.
- [5] Jiang J., Yaghi O.: Chem. Rev., 2015, **115**, 6966. <https://doi.org/10.1021/acs.chemrev.5b00221>
- [6] Jiang J., Gandara F., Zhang Y. *et al.*: J. Am. Chem. Soc., 2014, **136**, 12844. <https://doi.org/10.1021/ja507119n>
- [7] Sun Q., Hu K., Leng K. *et al.*: J. Mater. Chem. A, 2018, **6**, 18712. <https://doi.org/10.1039/C8TA06516K>
- [8] Prudius S., Melezhyk O., Brei V.: Stud. Surf. Sci. Catal., 2010, **175**, 233. [https://doi.org/10.1016/S0167-2991\(10\)75031-X](https://doi.org/10.1016/S0167-2991(10)75031-X)
- [9] Inshina O., Korduban A., Tel'biz G., Brei V.: Adsorpt. Sci. Technol., 2017, **35**, 439. <https://doi.org/10.1177/0263617417694887>
- [10] Bosman H., Kruissink E., Vanderspoel J., Vandenberg F.: J. Catal., 1994, **148**, 660. <https://doi.org/10.1006/jcat.1994.1253>
- [11] Tanabe K.: Solid Acid and Bases. Their Catalytic Properties. Academic Press, New-York-London 1970.
- [12] Tanabe K., Misono M., Hattori H., Ono Y.: New Solid Acids and Bases – Their Catalytic Properties, 1st edn. Elsevier Science, Amsterdam 1989, 124.
- [13] Barton D., Shtein M., Wilson R. *et al.*: J. Phys. Chem. B, 1999, **103**, 630. <https://doi.org/10.1021/jp983555d>
- [14] Rajagopal S., Nataraj D., Khyzhun O. *et al.*: Cryst. Eng. Comm., 2011, **13**, 2358. <https://doi.org/10.1039/C0CE00303D>
- [15] Khalamejda S., Samsonenko M., Sydoruk V. *et al.*: Theor. Exp. Chem., 2017, **53**, 40. <https://doi.org/10.1007/s11237-017-9499-5>
- [16] Manjunathan P., Marakatti V., Chandra P. *et al.*: Catal. Today, 2018, **309**, 61. <https://doi.org/10.1016/j.cattod.2017.10.009>

- [17] Bhagwat M., Shah P., Ramaswamy V.: Mater. Lett., 2003, **57**, 1604. [https://doi.org/10.1016/S0167-577X\(02\)01040-6](https://doi.org/10.1016/S0167-577X(02)01040-6)
- [18] Corma A., Nemeth L., Renz M., Valencia S.: Nature, 2001, **412**, 423. <https://doi.org/10.1038/35086546>
- [19] Moulder J., Stickle W., Sobol P., Bomben K.: Handbook of X-ray Photoelectron Spectroscopy, 1st edn. Perkin-Elmer Corporation Physical Electronics Division, USA 1992.
- [20] Guittet M., Crocombette J., Gautier-Soyer M.: Phys. Rev. B, 2001, **63**, 125117. <https://doi.org/10.1103/PhysRevB.63.125117>
- [21] Botella P., Corma A., Lopez-Nieto J. et al.: J. Catal., 2000, **195**, 161. <https://doi.org/10.1006/jcat.2000.2971>

Received: September 25, 2020 / Revised: October 05, 2020 /
Accepted: November 12, 2020

СУПЕРКИСЛОТНИЙ $ZrO_2-SiO_2-SnO_2$ ЗМІШАНИЙ ОКСИД: СИНТЕЗ ТА ДОСЛІДЖЕННЯ

Анотація. Суперкислотні потрійні $ZrO_2-SiO_2-SnO_2$ оксиди ($H_0 = -14.52$) синтезовано золь-гель методом з атомним співвідношенням в межах: $20 \leq Zr^{4+} \leq 29$, $60 \leq Si^{4+} \leq 67$, $11 \leq Sn^{4+} \leq 20$ ат. %. Суперкислотність $ZrO_2-SiO_2-SnO_2$ оксиду пояснена формуванням координаційно-ненасичених Zr^{4+} йонів, як сильних центрів Льюїса.

Ключові слова: тверда суперкислота, потрійний оксид, діоксид олова, сила кислотних центрів, центри Льюїса.